J. R. Clark, A.-C. Wong, and C. T.-C. Nguyen, "Parallel-resonator HF Micromechanical Bandpass Filters," *Digest of Technical Papers*, 1997 International Conference on Solid-State Sensors and Actuators, Chicago, Illinois, June 16-19, 1997, pp. 1161-1164.

Parallel-Resonator HF Micromechanical Bandpass Filters

John R. Clark, Frank D. Bannon III, Ark-Chew Wong, and Clark T.-C. Nguyen
Center for Integrated Sensors and Circuits
Department of Electrical Engineering and Computer Science, 2406 EECS Bldg.
University of Michigan
Ann Arbor, Michigan 48109-2122 USA
email: ctnguyen@eecs.umich.edu

SUMMARY

High frequency, fourth-order, micromechanical bandpass filters, with tunable frequency and bandwidth, and filter *Q*'s in the thousands, are demonstrated in a polysilicon surface micromachining technology. These filters utilize a parallel-resonator architecture, in which properly phased outputs from two or more micromechanical resonators are combined to yield a desired filter spectrum. Design formulas are given for Butterworth, Chebyshev, and Bessel filters, and each of these filter types are demonstrated with center frequencies close to 14.5 MHz and filter *Q*'s ranging from 830 to 1600.

Keywords: resonator, filter, communication

I. INTRODUCTION

The recent explosion in the demand for wireless capabilities has spurred great interest in the miniaturization of transceivers used in wireless networks. Historically, the size of the off-chip SAW and ceramic components used for frequency selection and reference generation in heterodyning transceivers has long been one of the major bottlenecks against miniaturization. As a result, the majority of approaches to miniaturization have explored alternative transceiver architectures, that do reduce the number of off-chip components, but suffer in performance [1]. Very recently, however, an alternative strategy for transceiver miniaturization has surfaced, in which high performance heterodyning architectures are retained, and miniaturization is achieved by replacing the aforementioned off-chip, high-*Q* mechanical resonator components with IC-compatible, micromechanical versions. To this end, a fourth-order, 8.37 MHz, spring-coupled micromechanical bandpass filter was recently demonstrated, with a filter *Q* of 340 and an associated insertion loss of less than 5 dB [2].

This paper describes an alternative mechanical filter architecture in which constituent micromechanical resonators are coupled electrically, rather than mechanically. By dispensing with rigid mechanical spring coupling, this parallel-resonator filter architecture both alleviates fabrication complexity associated with coupling springs (which often require submicron resolution for small filter bandwidths), and introduces real-time reconfigurability and bandwidth-tuning capabilities previously unavailable with spring-coupled architectures. After a brief introduction to parallel-resonator filter operation, this paper presents design equations for a variety of fourth-order bandpass filters, then verifies them via fabrication and testing of prototype bandpass filters centered at 14.5 MHz.

II. FILTER ARCHITECTURE AND OPERATION

Figure 1 presents the perspective view schematic of this parallel filter architecture, identifying key components and specifying the required bias and excitation scheme for proper filter operation. As shown, this filter is comprised of two HF micromechanical clamped-clamped beam resonators [2] ("μresonators"), fabricated side-by-side, with identical geometries and vibrational resonance frequencies. Conductive strips underlie the central regions of each resonator and serve as capacitive transducer electrodes. The resonator beams are suspended 1000Å above the substrate and electrodes, and are electrically connected together via a conductive strip, which also serves as the output electrode for this device.

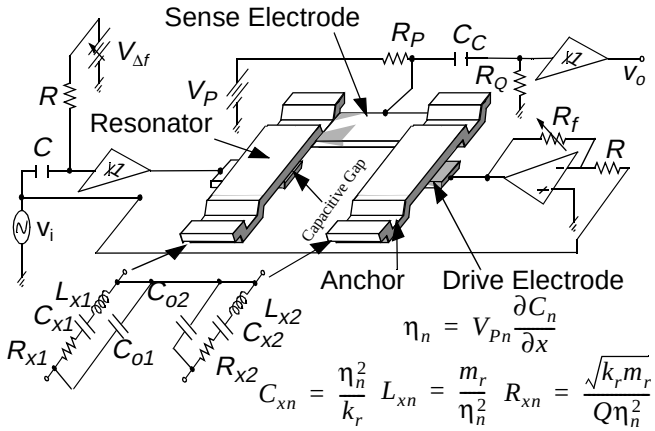

Fig. 1: Parallel-resonator filter schematic, showing biasing and excitation scheme, and identifying key components.

Under normal filter operation, a dc-bias voltage V_P is applied to each resonator through large resistor R_P, and buffered ac voltage input signals of opposite polarity, v_i and $-v_i$, are applied to each of the underlying electrodes. When the frequency of the applied ac input signal v_i enters the passband of one or both of the constituent resonators, the resonator(s) vibrate in a direction perpendicular to the substrate, creating dc-biased time varying capacitors between the resonators and their respective underlying electrodes. Currents are thus generated between the electrodes and resonators, given by $i_{xn}=V_{Pn}(\partial C_n/\partial t)$, where V_{Pn} is the dc voltage between resonator and electrode at port *n*, and C_n is the electrode-to-resonator overlap capacitance at port *n*. The currents from both resonators are then summed at the common output node and directed through ac coupling capacitor C_c into sense resistor R_Q, which then converts the current to an output voltage.

The mechanical resonators comprising the filter can be modelled in the electrical domain via electromechanical analogy, where each mechanical resonator corresponds to an equivalent series LCR circuit. The equivalent circuit representing the filter and electrode configuration is also shown in Fig. 1, along with equations for the elements. Using this circuit in combination with the electronics in Fig. 1, the filter is seen to operate via combination of the properly phased current outputs of the individual resonators. As shown in Fig. 2, inputs v_i at frequencies between the resonances of the microresonators generate output currents that are in phase, and thus, add, creating a flat passband in this frequency range. Those at frequencies outside this interval generate output currents 180^o out of phase, which subtract

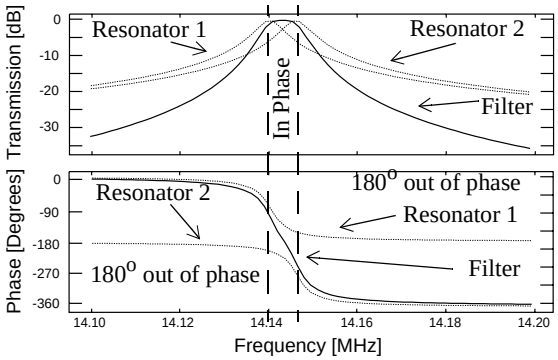

Fig. 2: Spectra depicting the mechanism behind filter operation.

to provide a steeper roll-off and improved stopband rejection. As shown, a two-resonator filter made in this manner provides a fourth-order bandpass characteristic. Higher order filters, with sharper roll-offs and larger stopband rejections, can also be implemented using the same principles with a larger number of micromechanical resonators.

III. PARALLEL-RESONATOR FILTER DESIGN

A. General Filter Design

The design of a given filter often begins with specification of a polynomial transfer function that approximates the desired filter characteristic. For a given filter order, the approximating polynomial generally takes on a specific form, which differs for the various filter types (i.e., Butterworth, Chebyshev, Bessel, etc.) only in the values of certain coefficients. For the particular case of the fourth-order (i.e., two-pole) bandpass filters of main interest here, the approximating polynomial takes the form

$$H(s) = \frac{As^2}{s^4 + as^3 + bs^2 + cs + \omega_o^4} \tag{1}$$

where ω_o is the center frequency of the filter, and the coefficients A, a, b, and c are functions of the filter type, as well as of the center frequency f_o and of filter quality factor Q_f. Normalized values for of these coefficients are readily available from data tabulated in filter cookbooks [3].

As mentioned, the output for the described parallel-resonator filter is derived by summing the properly phased current outputs of its constituent resonators. Given that each resonator realizes a second-order bandpass biquad voltage-to-current transfer function of the form

$$\frac{i_o}{v_i} = \frac{s(\omega_o/Q)}{s^2 + s(\omega_o/Q) + \omega_o^2}, \tag{2}$$

where ω_o is the radian center frequency, and Q is the quality factor of the resonator, the output of the filter may then be written as

$$\frac{i_o}{v_i} = \frac{\omega_1 - \omega_2}{Q_r} \frac{s(s^2 - \omega_1\omega_2)}{[s^2 + s(\omega_1/Q_r) + \omega_o^2][s^2 + s(\omega_2/Q_r) + \omega_o^2]} \tag{3}$$

where ω_n is the resonant frequency of resonator n and the Q's of each resonator are assumed to have the same value, Q_r. Comparing (3) with (1), it is apparent that the numerators cannot be made to match. This is of little consequence, however, since the numerator is still of lower order than the denominator, and thus, it still introduces loss poles only at zero and infinity.

By expanding the denominator in (3) and equating coefficients of like powers of s with those in (1), expressions for the

Table I: Filter Approximation Coefficients

Butterworth (maximally flat) $\alpha = 1,\ \delta = \sqrt{2}$ $\beta = \sqrt{1 + 16Q_f^2}$ $\theta = 2(1 + \beta)$
Chebyshev (equiripple) w/ 1 dB ripple $\alpha = 1.103,\ \delta = 1.098$ $\beta = \sqrt{1.217 + 16Q_f^4 + 4Q_f^2}$ $\theta = \beta(2.43 + 4Q_f^2) + 2.68 + 35.30Q_f^4 + 8.83Q_f^2$
Bessel (Linear Phase) $\alpha = 3,\ \delta = 1.098$ $\beta = \sqrt{9 + 16Q_f^4 - 12Q_f^2}$ $\theta = \beta(18 - 12Q_f^2) + 54 + 96Q_f^4 - 72Q_f^2$

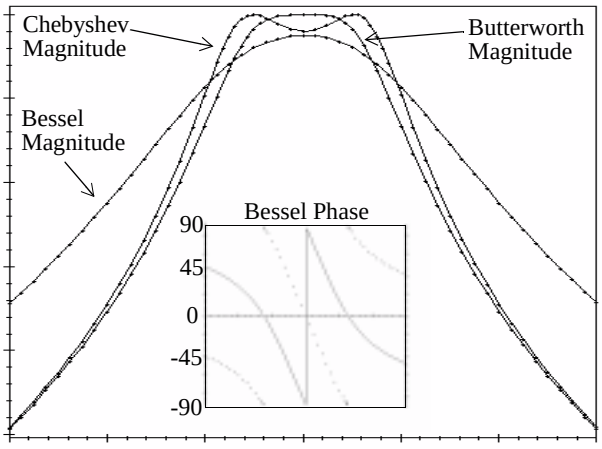

Fig. 3: Basic passband filter types and their approximations according to (3), (4), (5) and (6).

constituent resonator center frequencies (f_n's) and Q's required to implement a given filter characteristic can be derived. Doing so yields:

$$f_1 = \frac{2Q_f f_o}{\sqrt{\alpha + \beta + \sqrt{\theta/\beta}}} \tag{4}$$

$$f_2 = f_o^2/f_1 \tag{5}$$

$$Q_r = \frac{(f_1 + f_2)}{\delta f_o} Q_f \tag{6}$$

where Q_f and f_o are the Q and center frequency of the filter, and the new denormalized coefficients α, β, θ, and δ, once again depend on the type of filter. Table I summarizes these parameters for maximally-flat Butterworth, 1 dB equiripple Chebyshev, and linear-phase Bessel filters. Given desired filter parameters, f_o and Q_f, a straight forward application of (4), (5), and (6) yields a parallel-resonator filter design in terms of f_1, f_2, and Q_r.

Figure 3 presents plots of ideal filter spectra (dots) along with filter approximations given by (3), (4), (5), and (6) (solid line) for each of the filter types summarized in Table I. The

Table II: Resonator Design Data

Parameter	Value	Parameter	Value
L	30 μm	h	2 μm
W	8 μm	d	.1 μm
C_{on}	7.1 fF	dC/dx	70.8 nF/m
m_r	$4.4\text{x}10^{-13}$kg	k_r	3633 N/m
L_x	54.6 mH	C_x	2.20 fF
R_x	3.12 kΩ	η	$2.83\text{x}10^{-6}$

phase of the Bessel filter is also plotted. As shown in Fig. 3, the shapes of all three approximations are indistinguishable from the ideal filters within the passbands, although the Bessel filter does show a 90^o phase shift from ideal. Also, the approximation curves in Fig. 3 have been shifted vertically for better visual comparison of shapes with the ideal filter responses. In actuality, the Chebyshev and Bessel filters do suffer from some inherent insertion loss over the ideal cases. In the case of the Chebyshev filter, the insertion loss is equal to the amount of ripple, and for the Bessel filter it is approximately 1.25 dB.

B. Resonator Design

As seen from the above discussion, the frequency response of a parallel-resonator filter is determined primarily by the resonance frequency and Q's of its constituent resonators. For the case of clamped-clamped beam resonators with negligible axial stress, the resonance frequency is determined largely by geometry and material properties, and is given by

$$f_o = \frac{1}{2\pi}\sqrt{\frac{k_r}{m_r}} = 1.03\frac{h}{L^2}\sqrt{\frac{E}{\rho}} \tag{7}$$

where k_r and m_r are the respective spring constant and mass of the beam, h is the thickness, L is the length, E is the Young's modulus of the structural material, and ρ is its density. As thickness h is determined by the process, the length L represents the main design variable. Table II summarizes the relevant physical design data for resonators used in the filters of this work.

As mentioned, these filters are intended to be reconfigurable, in both type of response and bandwidth. Thus, rather than designing constituent resonators with a predetermined frequency separation, the resonators are made identical, and their frequency separation is adjusted after fabrication to meet the requirements of (4) and (5). Frequency tuning for this filter is achieved via the well-known electrostatic spring constant, k_e, that arises due to nonlinearity in the capacitive transducers [6], and that subtracts directly from the mechanical spring constant k_r in (7). The amount of frequency shift from the nominal mechanical resonance frequency is governed by the equation

$$f_o' = f_o\left(1 - \frac{V_{Pn}^{\ 2}C_{on}}{k_m d^2}\right)^{\frac{1}{2}}, \tag{8}$$

where f_o is the purely mechanical resonance frequency, and f_o' is the modified resonance frequency. Separate tuning of the resonators is achieved by applying a dc offset $V_{\Delta f}$ to resonator 1 (c.f., Fig. 2), resulting in a net bias voltage of V_P - $V_{\Delta f}$, which then separates the frequency of the resonators by

$$\Delta f = -\frac{1}{2}\frac{V_{\Delta f}^2 C_{on}}{k_m d^2} f_o \ . \tag{9}$$

Finally, the bandwidth of a given filter is set by R_Q, which effectively loads the Q's of the constituent resonators. To satisfy (6) for a given filter, R_Q should be chosen as

$$R_Q = R_x\left[\frac{Q_{res}}{Q_r} - 1\right], \tag{10}$$

where Q_{res} is the unloaded quality factor of the constituent resonators, and R_x is defined in Fig. 1.

Once the values of R_Q and R_x have been determined, the filter insertion loss readily follows and is determined by the resistive divider between R_x and R_Q:

$$IL = 20\log\left(\frac{R_Q}{R_Q + R_x}\right) \tag{11}$$

IV. EXPERIMENTAL RESULTS

Side-by-side resonators suitable for parallel-resonator filter implementation were designed to the specifications of Table II and fabricated using a $POCl_3$-doped, polysilicon surface-micromachining process [2]. The scanning electron micrograph (SEM) for a 14.5 MHz pair of resonators is presented in Fig. 6. Die containing the resonator pairs were then attached to a printed circuit board containing the output electronics and bonded directly to it. Careful layout procedures were followed to minimize parasitics. The pc board was placed in a custom-built vacuum chamber and pumped down to pressures on the order of 10 μTorr using a turbomolecular pump, and transmission spectra were taken using an HP4195A Network Analyzer.

Figure 5(a) shows the measured spectrum for a single resonator at 14.5 MHz. The extracted Q here is 1600, which is low for polysilicon resonators, but is consistent with recent data showing substantially lower Q for $POCl_3$-doped versus

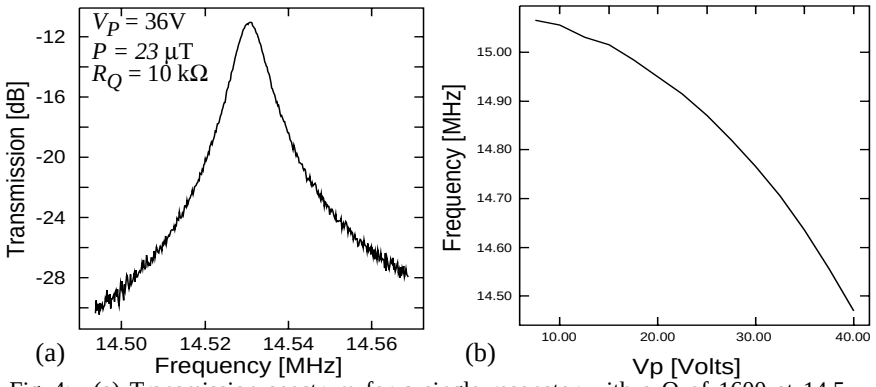

Fig. 4: (a) Transmission spectrum for a single resonator with a Q of 1600 at 14.5 MHz. (b) Plot of resonator frequency versus bias voltage.

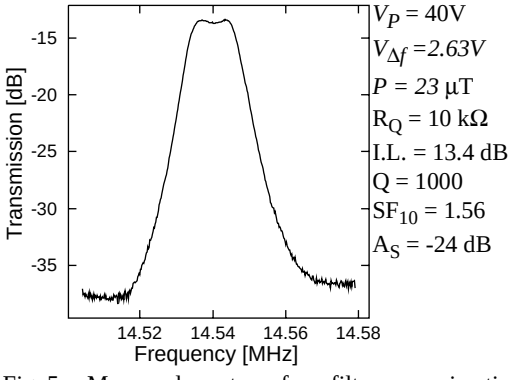

Fig. 5: Measured spectrum for a filter approximating a Butterworth function with R_Q = 10 kΩ

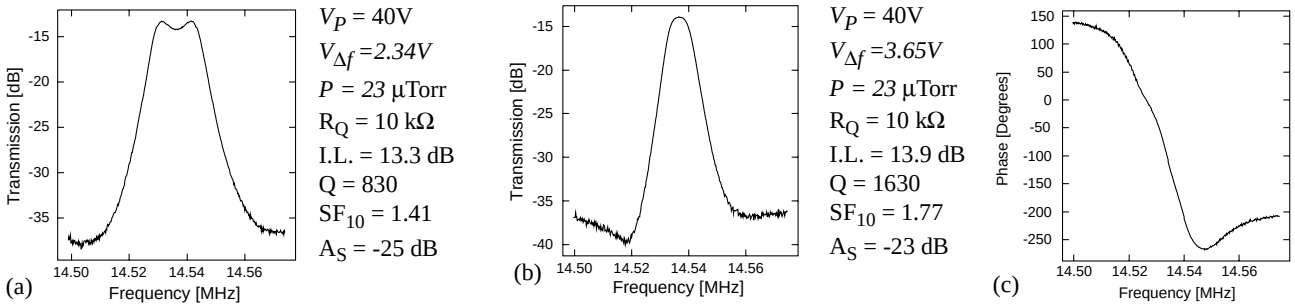

Fig. 7: Measured filter transmission spectra for (a) a Chebyshev approximation and (b) a Bessel approximation with its associated phase (c).

implant-doped polysilicon resonators [7]. Figure 5(b) shows a plot of resonator center frequency versus the tuning bias voltage V_P, and indicates a tunable frequency range of 500 kHz, or 3.4%.

Figure 6 shows the measured transmission spectrum for a parallel-resonator filter configured to a maximally flat (Butterworth) response centered at 14.54 MHz. The measurement was made at 23 mTorr, with V_P = 40V, $V_{\Delta f}$ = 2.63V, v_i=5mV, and R_Q = 10kΩ. The resulting filter Q is 1000 with 13 dB insertion loss (I.L.) and 24 dB of stopband rejection (A_s). Figures 7(a) and (b) present more spectra for the same pair of resonators, this time configured to a 1 dB ripple Chebyshev filter and a linear phase Bessel filter, respectively. In addition, the phase of the Bessel filter is given in Fig. 7(c), and relevant performance data are provided throughout the figure.

Two problems became apparent during testing. The first was the high insertion loss shown in Figures 6 and 7(a) and (b). For R_x = 3.12 kΩ and R_Q = 10 kΩ, the insertion loss estimated by (11) is 2.36 dB—much lower than the measured insertion loss. The second problem involved an inability to control the Q's of the constituent resonators via changes in R_Q. The filter Q's shown in Fig. 7 are well above the theoretically calculated and simulated values for R_Q=10kΩ, which were as low as 230 for maximally flat passbands.

Both of the above phenomena are largely a result of parasitic capacitance in parallel with R_Q, as shown in Fig. 8, which plots simulated frequency spectra for the case of (1) a filter terminated with R_Q = 10 kΩ; (2) another terminated with R_Q = 10 kΩ in parallel with a 5pF capacitor; and (3) another terminated as in case (2), but frequency-tuned to achieve a flat passband. Note that the bandwidth in (3) must be significantly reduced to achieve a flat passband, and this then introduces additional

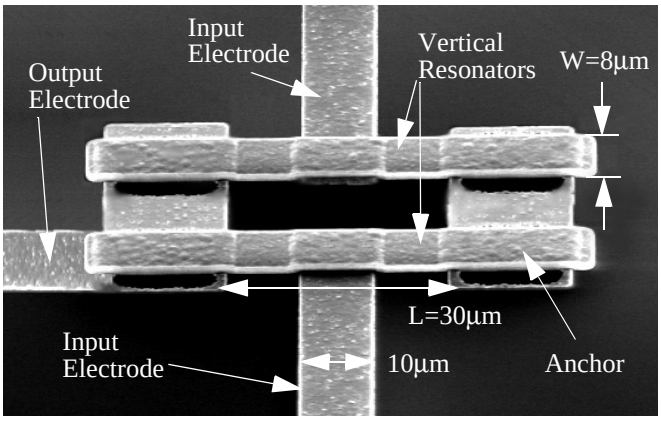

Fig. 6: SEM of a 14.5 MHz parallel filter with critical dimensions labeled.

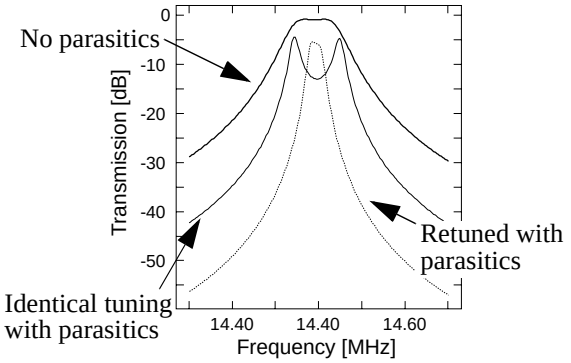

Fig. 8: Transmission spectra showing the effect of parasitic capacitance in parallel with R_Q.

insertion loss. The effective filter bandwidth shrinks mainly because parasitic capacitance in parallel with R_Q reduces the total resistance seen in shunt with the output, thus, reducing Q-loading ability of R_Q. In addition, shunt parasitic capacitance also introduces a low frequency pole, causing the frequency response of the circuit to roll-off prematurely. SPICE simulations indicate that this can be a dominant mechanism by which insertion loss is degraded.

V. CONCLUSIONS

Fourth-order, reconfigurable, micromechanical bandpass filters based on a parallel-resonator architecture have been demonstrated in a polysilicon surface-micromachining technology. Using this filter topology, a single pair of clamped-clamped beam micromechanical resonators were configured to approximate a variety of fourth-order filter types, including the popular Butterworth, Chebyshev, and linear phase Bessel filters.

The filters of this work were found to be greatly affected by off-chip parasitic capacitance, which reduced the maximum achievable bandwidth and greatly increased the insertion loss of these passive filters. More careful board layout or full integration of circuits and micromechanical resonators are two possible methods for alleviating the effect of parasitics.

VI. REFERENCES

[1] A. A. Abidi, *IEEE J. Solid. State. Circuits, vol. 30, No. 12, pp 1399-1410, Dec. 1995.*

[2] F.D. Bannon, et al., *IEDM Tech. Digest*, pp. 773-776.

[3] A. I. Zverev, *Handbook of Filter Synthesis*, 1967.

[4] H. Khorramabadi et al., *IEEE J. Solid. State. Circuits*, Vol. SC-18, pp. 644-651, Dec. 1983.

[5] C.T.-C. Nguyen et al., *IEDM Tech. Digest*, pp. 505-508, 1992.

[6] H. Nathanson, et. al., *IEEE Trans. Electron Devices*, vol. ED-14, No. 3, pp. 117-133, March 1967.

[7] K. Wang, et al., *Tech. Digest*, Transducers'97, 1997.